Stress Analysis of Dental Implant System Using Homogenization Technique

Jinhee Lee, Ph.D.*, Chul-Su Koh, D.D.S., M.S.D.**, and Kuiwon Choi, Ph.D.***

ABSTRACT

A stress analysis of dental implant system is carried out using homogenization technique. Homogenization technique helps make proper material model of bone and analyze such a nonhomogeneous structure at the level of individual microstructural unit. The computed stress state based on it is found by an order of magnitude higher than that of a conventional finite element model. It also manifests that even a minor lateral force results in crucial stresses in the dental implant system and that the macroscale model should take the shape and size after real mandible to produce reasonable solutions.

INTRODUCTION

The advant of osseointegrated implants in the mid-seventies has revolutionized prosthodontic care. The attraction to endosseous implants lies in the potential for improved function over standard removable dentures, improved esthetics, and more favorable stress distribution in the bone. Periodontally compromized individuals can also have dentition stabilized with implants support for a better long term prognosis. It is reported the overall success rate of implant system has been a lot more than 80 percents. However, endosteal dental implants can induce resorption in the surrounding bones leading to gradual loosening and ultimately to complete loss of the implant. Since high stress in the dental implant system causes bone resorption, connective tissue ingrowth and subsequent failure, it is very important to identify the stress levels in the jaw bone when dental implant system is inserted and is subject to occlusal loading.

Finite element method (FEM) has reigned as one of the most powerful tools in the area of stress analysis. FEM offers the potential of evaluating and improving implant design without the risk and expense of surgery. Eventhough there has been numerous use of the FEM modeling technique in the design and evaluation of dental implants, few attempts have been made to relate the computational models to those mechanical and

* Assistant Professor, Department of Machine Design and Mechanics, Hong-Ik University

** Departmente of Periodontology, School of Dentistry, Kyung-Hee University

*** Senior Research Scientist, Biomedical Research Center, KIST

histological data obtained from actual specimens.

Numerous studies which tried to compute the stress distributions in the implant system with FEM have been reported. Tesk[16], Privitzer[9], and Takahashi[15] are among those who introduced the concept of stress analysis using finite element method to implant dentistry. Siegel *et al.*[14], French *et al.*[4] and Rieger *et al.*[10-13] conducted series of stress analyses on implant systems where they compared and evaluated various implant designs using two-dimensional and axisymmetric finite element models. Knoell[5], Brocher *et al.*[1], and Cook *et al.*[3] presented three-dimensional finite element models of stress distribution in the bone.

Although many previous studies with conventional FEM helped identify various biomechanical aspects of implant functions, it is worth while to note that FEM is based on the continuum mechanics and to check whether those modelings satisfy the basic assumptions concernig the geometric characteristics of bone microstructures. In this study a stress analysis of mandible with a dental implant of rectangular cross section is carried out using homogenization technique to enhance the accuracy of stress computations of the dental implant system.

ANALYSIS

A close look at the sponge bone microstructure reveals that it is extremely difficult to analyze such a structure at the level of individual microstructural units. The application of FEM using coarse meshes also imposes several intrinsic difficulties in this case. Conventional FEM assumes material homogeneity and isotropy, and it is apparent that such assumptions are hardly applicable to the stress analysis of bone because of the high degree of material heterogeneity of the bone microstructure. Lavernia *et al.*[8] tried a finite element analysis in which a trabecular model was presented for cancellous bone, even though they did not provide a systematic approach.

One of the reasonable ways to overcome this difficulty is to find equivalent material model without a need to represent each and every individual microstructural unit. The homogenization technique, which introduces asymptotic expansion to the standard FEM, helps find such a material model which is able to characterize the average mechanical behavior as well as represent the effect of the material heterogeneities. (ref. Appendix) Ko *et al.*[6] and Kohn *et al.*[7] applied homogenization technique in their studies to compute the stress levels around dental implants.

The geometric complexity of the sponge bone is the major obstacle to the stress analysis. Even though it is almost impossible to identify its geometry accurately, it is generally accepted that the bone has interconnected branch-like structure and that the bone density is about 0.3. Instead of assuming that the sponge bone is a homogeneous material as in the conventional FEM, homogenization technique models the sponge bone to have a *unit cell* that repeats itself in every direction to form the entire structure. Fig. 1 shows a finite element mesh (40 QUAD8 elements) that represents a unit cell and the sponge bone model that is constructed by the repetition of the unit cell. The unit cell is constructed to account the bone density and is smoothly curved to avoid stress concentrations.

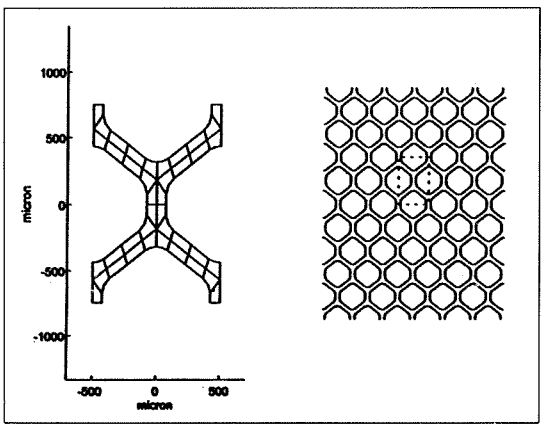

Fig. 1 Unit cell and sponge bone model

Table 1 Homogenized plane strain elasticity tensor E^H of sponge bone (MPa)

Sponge bone	549.825	468.169	0.
	468.169	632.170	0.
	0.	0.	155.044

Table 2 Plane strain elasticity tensors of cortical bone and titanium (MPa)

Cortical bone	22884.61	9807.69	0.
	9807.69	22884.61	0.
	0.	0.	6538.46
Titanium	162980.98	80274.21	0.
	80274.21	162980.98	0.
	0.	0.	41353.38

Two kinds of plane strain models, model A and model B, are tried in this study. The purpose of the model A is twofold: to demonstrate how the homogenization technique works and to show how much the results of such a oversimplifed model deviate from those of more reasonable model, say, model B. Model A is composed of 23㎜ of sponge bone layer and 2㎜ of cortical bone layer which is rigidly attached on the sponge bone layer. A dental implant of 4㎜ diameter and 12㎜ length is embedded 10㎜ into the cortical-sponge bone complex as shown in Fig.2 and Fig.3. Experimental results indicate that Young's modulus and Poisson's ratio of bone is about 5 GPa and 0.3, respectively[2]. The plane strain elasticity tensor of sponge bone is computed using eq.(A16) and is given in Table 1. Also given in Table 2 are the plane strain elasticity tensors of cortical bone and

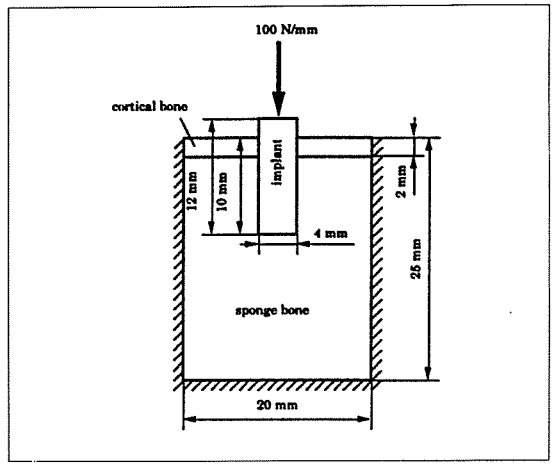

Fig. 2 Model A, load case 1

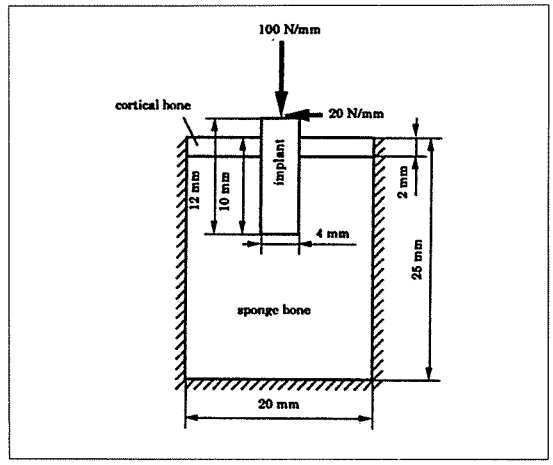

Fig. 3 Model A, load case 2

titanium whose Young's moduli are rated as 17 GPa (ν=0.3) and 110 GPa (ν=0.34), respectively. Two load cases for model A are chosen to show how much difference lateral force makes to the stress distributions in the mandible. Compressive force of 100 N/㎜ is applied at the top center of the dental implant for the load case 1 (Fig.2), while lateral force of 20N/㎜ along with 100N/㎜ compressive force is applied for the load case 2 (Fig.3). It is important to note that the macroscale displacement field should be provided to compute the microscale stresses in homogenization techni-

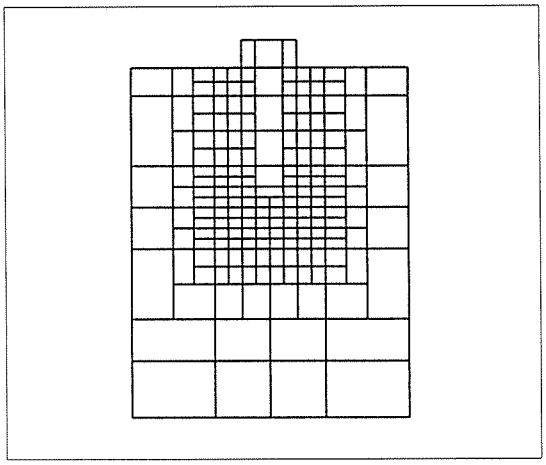

Fig. 4 Finite element mesh for model A

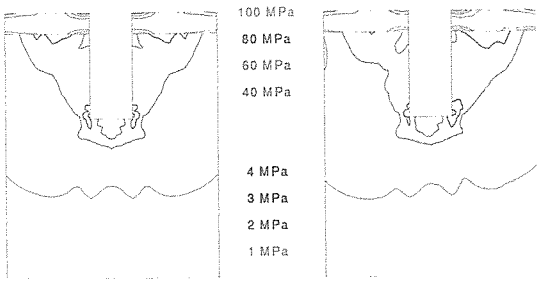

Fig. 5 Macroscale stress (von Mises) of model A

que. The macroscale displacement field is obtained using conventional FEM with coarse mesh if homogenized material properties are used. A finite element mesh (190 QUAD8 elements, 647 nodes) as shown in Fig.4 is used to compute the macroscale displacement fields of model A of Fig.2 and Fig.3, and the results are shown in Fig.5 as projected equivalent stresses in macroscale.

A cursory look at Fig.5 reveals that the stress levels of cortical bone are much higher than those of sponge bone in macroscale. It appears that the stress state of cortical bone is due to beam bending mode, i.e., the cortical bone bears most of the applied load and the load carrying capacity of

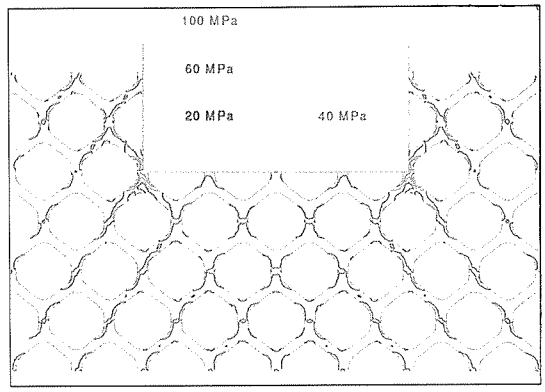

Fig. 6 Microscale stress (von Mises) of model A, load case 1

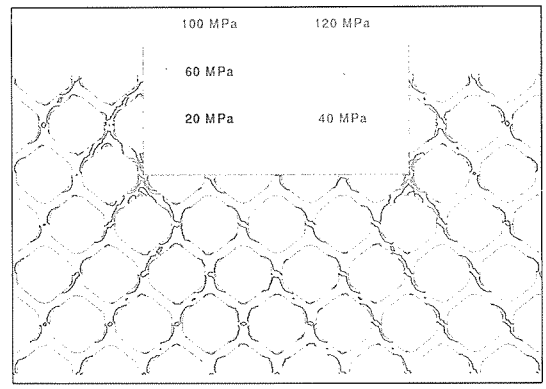

Fig. 7 Microscale stress (von Mises) of model A, load case 2

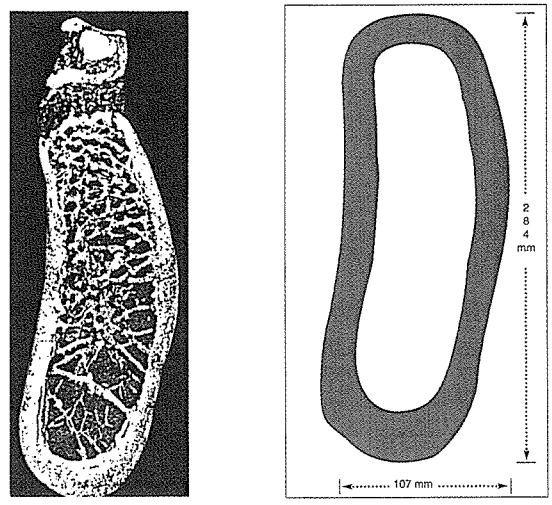

Fig. 8 Cross section of a mandible (P2)

sponge bone is very poor. Even though there is a little change in the stress pattern when lateral force as well as compressive force is applied to the implant as seen in Fig.5, it is likely that the presence of 20% of lateral force does not make much difference in model A. Once the displacements are given in macroscale, microscale stresses are computed using eq.(A17). Shown in Fig.6 and Fig.7 are the projected microscale stress fields of sponge bone around the implant tips where stress level in Fig.5 are relatively high.

As seen in Fig.5 through Fig.7, the computed stress levels of sponge bone using homogenization technique reveal huge differences, upto 30 times, compared to results of conventional FEM. The fundamental assumption of conventional method is to identify the sponge bone as a homogeneous continuum, which is not appropriate since the actual analyses are not carried out at the level of individual microstructural units. Consequentely, the resulted macroscale stresses of Fig.5 fail to describe what really happens in the microstructures of sponge bone. Above all, the fact that the sponge bone density is 0.3 and that the interconnected branch-like bone structure is more likely to lead to any form of stress concentration tells us that the sponge bone is much weaker than under the continuum assumption.

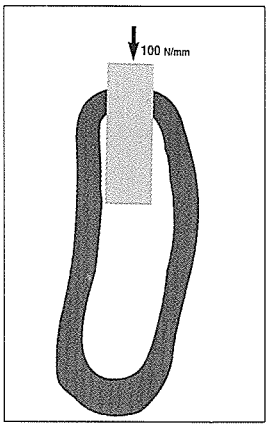

Fig. 9 Model B, load case 1

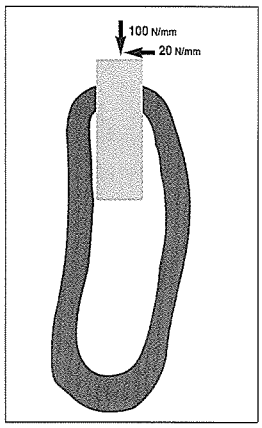

Fig.10 Model B, load case 2

Model B takes the shape and size after real mandible and, consequentely, is supposed to result in more reasonable solutions than those of model A. Fig.8 shows the cross section of a typical mandible at premolar 2 (P2) of which physical dimensions are found in Uejo[17]. The same implant as described in model A is embedded 10㎜ into the mandible and two kinds of load cases are applied at the top center of the implant: 100N/㎜ of compressive force for the load case 1 (Fig.9) and 20N/㎜ of lateral force along with 100N/㎜ compressive force (Fig.10). Fig.11 shows the finite element mesh (188 QUAD8 elements, 625 nodes) of model B. The macroscale displacements of model B are computed for each load case using conventional FEM as shown in Fig.12, from which the macroscale stresses of cortical bone and sponge bone are plotted in Fig.13.

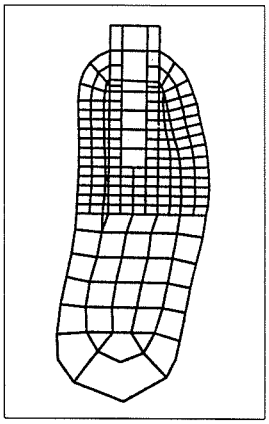

Fig.11 Finite element mesh for model B

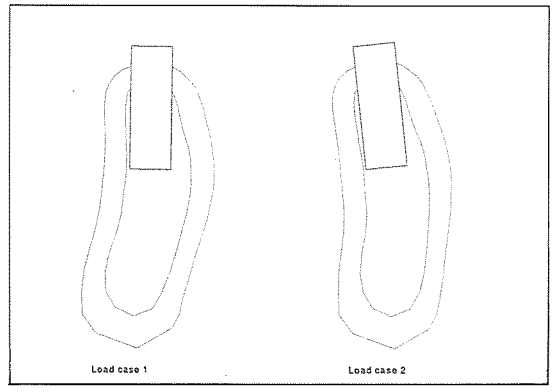

Fig.12 Macroscale displacements of model B (x10)

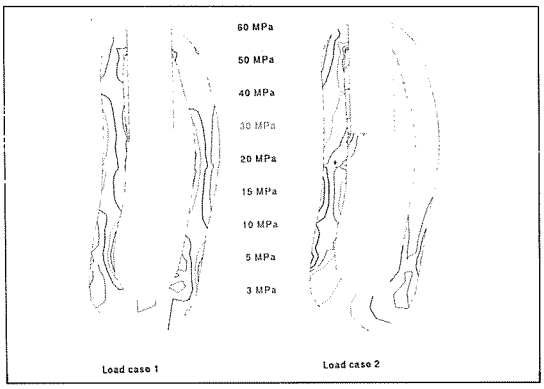

Fig.13 Macroscale stress 'von Mises' of model B

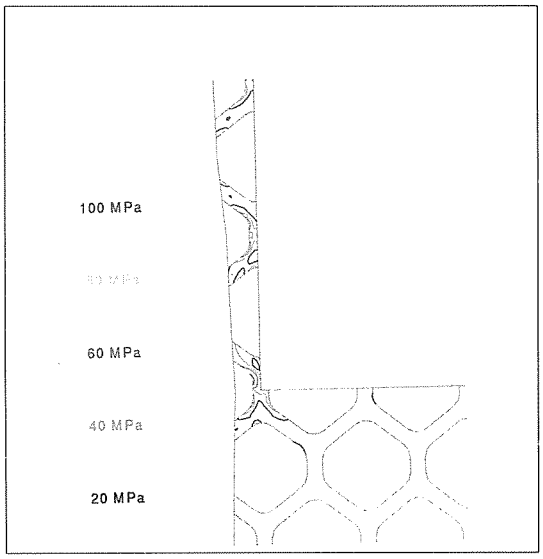

Fig.14 Microscale stress 'von Mises' of model B, load case 1

It is observed that the stress levels of Fig.13 differ drastically for each load case due to the presence of 20% of lateral force. It is shown in Fig .12 that the compressive force only (load case 1) actually compresses the mandible and bends it a little bit to the right while the effect of the compressive-lateral force (load case 2) is to bend the mandible to the left. It is also worth while to note that the relative displacement between the bottom left tip of the implant and left wall of cortical bone vary for each case. The applied forces given in load case 1 and load case 2 make the mandible-implant complex deform in so different ways that the resulted stress levels are totally different. The sponge bone is completely surrounded by 2 ㎜ thick cortical bone in model B, and it is likely that cortical bone bears most of the applied load and sponge bone passively undergoes deformation as discussed earlier.

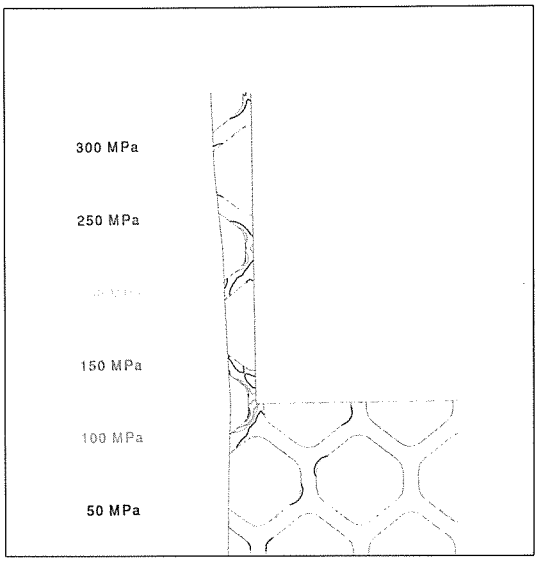

Fig.15 Microscale stress (von Mises) of model B, load case 2

Microscale stresses are calculated from the macroscale displacements using eq.(A17). Fig.14 and Fig.15 show the projected microscale stress fields of the sponge bone at the vicinity of the bottom left tip of implant where high stress concentrations exist.

As can be seen in Fig.12 through Fig.15, different loading conditions make wholly different displacement patterns and stress distributions in the mandible. Considering the fact that all the computations are made within the limits of linear analyses, it is clear that the lateral force is responsible for the moment that bends the mandible to the left and the excessive stresses of Fig.15. This explains the mechanism how lateral force damages the weak spot of mandible and shortens

the life of dental implant. It is also noted that the solutions of model A are less reasonable than those of model B and that the geometric information of a dental implant model should be sophisticated enough because one can not expect reasonable solutions from too much simplified models such as model A in this study.

DISCUSSIONS

By most researchers it has been believed that the occlusal loads are highly localized in the crestal region and that the bone resorption of the area is the most important criterion of failure in dental implant, partly because the radiologic results do not show radiolucency of early phase of sponge bone destruction. Consequently, attention is focused entirely on the cortical bone and sponge bone is considered to have no role in implant support.

However, the results of this study reveal some deviations from the existing concepts, which show higher stress levels in the sponge bone than that of cortical bone. It is likely that the initial bone destruction begins at the sponge bone around implant tip and the failure in sponge bone increases the burden of the cortical bone which causes implant failure eventually. The authors think that more reseaches should be carried out on the early phase of implant failure including the stress state of sponge bone for optimal design of dental implant systems and their applications.

CONCLUSIONS

1. Homogenization technique helps make proper material models which are able to characterize the average mechanical behaviors as well as to represent the effect of the material heterogeneities.
2. It is required that a model that takes the shape and size after real mandible be used in the stress analyses of dental implant since oversimplified model does not provide reasonable solutions.
3. The lateral force is responsible for the torque that bends the mandible and that causes the excessive stress in the mandible-implant system.

NOMENCLATURE

b_i	body force
E	elasticity tensor
E^H	homogenized elasticity tensor
t_i	traction
u_i,$\underline{u}$	displacement
v_i,$\underline{v}$	virtual displacement
x_i,$\underline{x}$	macroscale coordinate
y_i,$\underline{y}$	microscale coordinate
ν	Poisson's ratio
σ	stress
χ	microscale variable

APPENDIX

The finite element weak form of linear elasticity problem is given by

$$\int_\Omega E_{ijkl}\frac{\partial u_k}{\partial x_l}\frac{\partial v_i}{\partial x_j}d\Omega = \int_\Omega b_i v_i d\Omega + \int_\Gamma t_i v_i d\Gamma \quad (A1)$$

In homogenization theory, the field variables including virtual displacements are expressed as asymptotic expansions with respect to the parameter ε such that

$$\underline{u} = \underline{u}^0(\underline{x}) + \varepsilon \underline{u}^1(\underline{x}, \underline{y}) + O(\varepsilon^2) \quad (A2)$$

$$\underline{v} = \underline{v}^0(\underline{x}) + \varepsilon \underline{v}^1(\underline{x}, \underline{y}) + O(\varepsilon^2) \quad (A3)$$

hold, where $\underline{y} = \frac{\underline{x}}{\varepsilon}$ is the macroscale coordinates.

The gradients of u and v are:

$$\nabla \underline{u} = \nabla_{\underline{x}} \underline{u}^0 + \varepsilon \nabla_{\underline{x}} \underline{u}^1 + \nabla_{\underline{y}} \underline{u}^1 \quad (A4)$$

$$\nabla \underline{v} = \nabla_{\underline{x}} \underline{v^0} + \varepsilon \nabla_{\underline{x}} \underline{v^1} + \nabla_{\underline{y}} \underline{v^1} \quad \text{(A5)}$$

Substituting eq.(A2)-(A5) into eq.(A1) and rearranging gives

$$\int_\Omega E_{ijkl}\left(\frac{\partial u^0_k}{\partial x_l} + \frac{\partial u^1_k}{\partial y_l}\right)\left(\frac{\partial v^0_i}{\partial x_j} + \frac{\partial v^1_i}{\partial y_j}\right) d\Omega$$
$$+\varepsilon \int_\Omega E_{ijkl}\left\{\frac{\partial u^1_k}{\partial x_l}\left(\frac{\partial v^0_i}{\partial x_j} + \frac{\partial v^1_i}{\partial y_j}\right)\right.$$
$$\left.+\left(\frac{\partial u^0_k}{\partial x_l} + \frac{\partial u^0_k}{\partial y_l}\right)\frac{\partial v^1_i}{\partial x_j}\right\} d\Omega$$
$$+\varepsilon^2 \int_\Omega E_{ijkl}\frac{\partial u^1_k}{\partial x_k}\frac{\partial v^1_i}{\partial x_j} d\Omega$$
$$= \int_\Omega b_i(v^0_i + \varepsilon v^1_i) d\Omega + \int_\Gamma t_i(v^0_i + \varepsilon v^1_i) d\Gamma \quad \text{(A6)}$$

Taking the limit of $\varepsilon \to 0$ reduces eq.(A6) to

$$\lim_{\varepsilon \to 0} \int_\Omega E_{ijkl}\left(\frac{\partial u^0_k}{\partial x_l} + \frac{\partial u^1_k}{\partial y_l}\right)\left(\frac{\partial v^0_i}{\partial x_j} + \frac{\partial v^1_i}{\partial y_j}\right) d\Omega$$
$$= \lim_{\varepsilon \to 0}\left\{\int_\Omega b_i v^0_i d\Omega + \int_\Gamma t_i v^0_i d\Gamma\right\} \quad \text{(A7)}$$

Since the virtual displacement $v = \underline{v^0} + \varepsilon \underline{v^1}$ is arbitrary, it turn out that $\underline{v^0}$ and $\underline{v^1}$ are also arbitrary and eq.(A7) is rewritten as

$$\lim_{\varepsilon \to 0} \int_\Omega E_{ijkl}\left(\frac{\partial u^0_k}{\partial x_l} + \frac{\partial u^1_k}{\partial y_l}\right)\frac{\partial v^0_i}{\partial x_j} d\Omega$$
$$= \lim_{\varepsilon \to 0}\left\{\int_\Omega b_i v^0_i d\Omega + \int_\Gamma t_i v^0_i d\Gamma\right\} \quad \text{(A8)}$$

and

$$\lim_{\varepsilon \to 0} \int_\Omega E_{ijkl}\left(\frac{\partial u^0_k}{\partial x_l} + \frac{\partial u^1_k}{\partial y_l}\right)\frac{\partial v^1_i}{\partial y_j} d\Omega = 0 \quad \text{(A9)}$$

It is readily seen that eq.(A8) and eq.(A9) are not independent, rather they are mutually depedent through $\frac{\partial u^0_k}{\partial x_l} + \frac{\partial u^1_k}{\partial y_l}$.

Considering that the microscale integration can be replaced by a averaged-value integration for a general Y-periodic function Φ,

$$\lim_{\varepsilon \to 0} \int_\Omega \Phi(\underline{x}, \underline{y}) d\Omega = \int_\Omega \frac{1}{|Y|} \int_Y \Phi(\underline{x}, \underline{y}) dY\, d\Omega \quad \text{(A10)}$$

eq.(A8) and eq.(A9) are now modified to result in

$$\int_\Omega \frac{1}{|Y|} \int_Y E_{ijkl}\left(\frac{\partial u^0_k}{\partial x_l} + \frac{\partial u^1_k}{\partial y_l}\right)\frac{\partial v^0_i}{\partial x_j} dY\, d\Omega$$
$$= \int_\Omega b_i v^0_i d\Omega + \int_\Gamma t_i v^0_i d\Gamma \quad \text{(A11)}$$

and

$$\int_\Omega \frac{1}{|Y|} \int_Y E_{ijkl}\left(\frac{\partial u^0_k}{\partial x_l} + \frac{\partial u^1_k}{\partial y_l}\right)\frac{\partial v^1_i}{\partial y_j} dY\, d\Omega = 0 \quad \text{(A12)}$$

Considering the linear relationship, the following separation of variables is the sufficient condition to satisfy eq.(A12):

$$u^1_i(\underline{x}, \underline{y}) = -\chi^{pq}_i(\underline{y})\frac{\partial u^0_p(\underline{x})}{\partial x_q} \quad \text{(A13)}$$

The microscale variable χ is computed by the substitution of eq.(A13) into eq.(A12)

$$\int_Y \left(E_{ijkl} - E_{ijpq}\frac{\partial \chi^{kl}_p}{\partial y_q}\right)\frac{\partial v^1_i}{\partial y_j} dY \frac{\partial u^0_k}{\partial x_l} = 0 \quad \text{(A14)}$$

Finally the weak form of the macroscale eq. (A11) is rewritten as

$$\int_\Omega E^H_{ijkl}\frac{\partial u^0_k}{\partial x_l}\frac{\partial v^0_i}{\partial x_j} d\Omega = \int_\Omega b_i v^0_i d\Omega + \int_\Gamma t_i v^0_i d\Gamma \quad \text{(A15)}$$

where the homogenized elasticity tensor E^H and the microscale stress σ are computed by

$$E^H_{ijkl} = \frac{1}{|Y|} \int_Y \left(E_{ijkl} - E_{ijpq}\frac{\partial \chi^{kl}_p}{\partial y_q}\right) dY \quad \text{(A16)}$$

and

$$\sigma_{ij} = E_{ijkl}\left(\frac{\partial u^{0}_{k}}{\partial x_{l}} + \frac{\partial u^{1}_{k}}{\partial y_{l}}\right) + O(\varepsilon^{2}) , \qquad (A17)$$

respectively.

REFERENCES

1. Borcher, L. and Reichart, P.,"Three dimensional stress distribution around dental implant at different stages of interface development", J. Dent. Res., 1983, vol. 62, no. 2, pp 155-159
2. Choi, K., Kuhn, J.L., Ciarelli, M.J., and Goldstein, S.A., "The elastic moduli of human subchondral, trabecular, and cortical bone tissue and the size-dependency of cortical bone modulus", J. Biomechanics, 1990, vol. 23, no. 11, pp 1103-1113
3. Cook, S.D., Weinstein, A.M., and Klawitter, J.J., "A three-dimensional finite element analysis of a porous rooted Co-Cr-Mo alloy dental implant", J. Dent. Res., 1982, vol. 61, no. 1, pp 25-29
4. French, A.A., Bowles, C.Q., Parham, P.L., Eick, J.D., Killoy, W.J., and Cobb, C.M., "Comparison of peri-implant stresses transmitted by four commercially available osseointegrated implants", Int. J. Perio & Rest. Dent., 1989, vol. 9, pp 221-230
5. Knoell, A.C.,"A mathematical model of an in vitro human mandible", J. Biomechanics, 1977, vol. 10, pp 159-169
6. Ko, C.C., Kohn, D.H., and Hollister, S.J., " Micromechanics of implant tissue interfaces", J. Oral Implat., 1992, vol. 18, no. 3, pp 220-230
7. Kohn, D.H., Ko, C.C., and Hollister, S.J., "Localized mechanics of dental implants", BED -vol. 24, 1993, Bioengineering Conf., ASME, pp 331-334
8. Lavernia, C.J., Cook, S.D., Weinstein, A.M., and Klawitter, J.J., "An analysis of stresses in a dental system", J. Biomechanics, 1981, vol. 14, no. 8, pp 555-560
9. Privitzer, E., Wiedera, O., and Tesk, J.A., " Some factors affecting dental implant design", J. Biomed. Mater. Res. Symp., 1975, vol. 6, pp 251-260
10. Rieger, M.R., Adams, W.K., and Kinzel, G.L., "A finite element survey of eleven endosseous implants", J. Prosthet. Dent., 1990, vol. 63, no. 4, pp 457-465
11. Rieger, M.R., Adams, W.K., Kinzel, G.L., and Brose, M.O.,"Finite element analysis of bone-adapted and bone-bonded endosseous implants ", J. Prosthet. Dent., vol. 62, no. , pp 436-440
12. Rieger, M.R., Fareed, K., Adams, W.K., and Tanquist, "Bone stress distribution for three endosseous implants", J. Prosthet. Dent., 1989, vol. 61, no. 2, pp 223-228
13. Rieger, M.R., Mayberry, M., and Brose, M.O., "Finite element analysis of six endosseous implants", J. Prosthet. Dent., 1990, vol. 63, no. 6, pp 671-676
14. Siegel, D. and Soltész, U., "Numerical investigation of the influence of implant shape on stress distribution in the jaw bone", Int. J. Oral & Maxillofac. Implants, 1989, vol. 4, no. 4, pp 333-340
15. Takahashi, N., Kitagami, T., and Komori, T., " Analysis of stress on a fixed partial denture with a blade-vent implant abutment", J. Prosthet. Dent., 1978, vol. 40, no. 2, pp 186-191
16. Tesk, J.A. and Widera, O.,"Stress distribution in bone arising from loading on endosteal dental implants", J. Biomed. Mat. Res. Symp., 1973, vol. 4, pp 251-261
17. 上條雍彦, 口腔解剖學, 1 骨學 (頭蓋學), アナトーム社 ,1988

초 록

균질화기법을 적용하여 치과 임플란트 시스템에 대한 미세응력해석을 수행하였다. 균질화기법은 하악골내의 해면골과 같은 비균질 비등방성 구조체에 대한 물질모델을 설정하고 이를 이용하여 수치해석시 작은 계산량으로도 해면골조직의 미세단위까지의 응력해석을 가능케 하여준다. 균질화기법을 적용하여 계산된 해면골의 스트레스레벨은 기존의 방법으로 계산된 수치보다 열배이상 높게 나타났는데, 이는 치과 임플란트 시스템의 응력상태에 대한 기존의 인식과 큰 차이를 보이고 있어 치과 임플란트 설계에 대한 전반적인 검토가 필요한 것으로 생각된다. 또한 균질화기법을 통하여 임플란트 시스템에 대한 측방력의 효과는 매우 크게 나타남을 확인할 수 있었고, 임플란트 시스템의 응력해석시 지나치게 단순화된 유한요소 모델을 사용함으로서 발생되는 오류가 지적되었다.